# Design of an Endoscopic Biopsy Needle With Flexural Members

Stacy L. Figueredo

Massachusetts Institute of Technology, Precision Engineering Research Group, Cambridge, MA 02139

William R. Brugge

Massachusetts General Hospital, Gastrointestinal Endoscopy Unit, Boston, MA 02114

Alexander H. Slocum

Massachusetts Institute of Technology, Precision Engineering Research Group, Cambridge, MA 02139

As a minimally invasive means of extracting a tissue sample from a patient, current endoscopic biopsy needles generally do not preserve tissue histology and often require multiple attempts to obtain a tissue sample. This paper presents an endoscopic biopsy needle with internal flexures that enables tissue to enter the hollow needle and then be severed from the surrounding tissue when the needle is withdrawn. Using force-deflection and sample weight data from 10× scaled prototypes, variations of a flexural design captured 1.1 grams of a tissue phantom on average, as compared to wedge-type designs that averaged 0.7-0.8 grams. Sample mass exhibited an increase in mass as the feature angle decreased. Peak entrance forces (P2) for the flexure design were lower than for both wedge and extended wedge designs, and resistance forces (S2) were higher upon needle extraction. A low-angle (15 and 30 deg) feature also produced a lower entrance friction (S1) and higher exit resistance (S2) compared with 45 and 60 deg features. These results suggest that a biopsy needle with 15 deg flexures could increase sample length and mass as well as sampling success rates for core biopsy procedures. Future tests of the flexural biopsy needle design will use this information to determine dimensions for laser cut features of 1× scale needles. [DOI: 10.1115/1.2355693]

#### 1 Introduction

Gastrointestinal cancers are the most common malignancy in the United States, and cancer of the gastroesophageal junction is the most rapidly increasing cancer in the U.S. [1]. The vast majority of GI cancers are diagnosed with endoscopic instruments that provide high resolution video and ultrasound images. According to a National Health Statistics study taken in 1996, over 1.2 million endoscopic biopsies are performed in the United States each year [2]. Current endoscopic biopsy needle designs use a scooping-type mechanism and often require multiple attempts to acquire samples for cytological and histological analysis of tissues. The endoscopy procedure and endoscope designs place geometric constraints on the design of a needle biopsy device, such as the maximum needle diameter and minimum required sample length. Functional requirements are detailed in Fig. 1 [3–7].

This project aims to develop a safe and reliable endoscopic biopsy needle that will improve tissue sampling success rates by using flexural tip elements that allow tissue to enter the needle yet sever a sample from surrounding tissue as the needle is withdrawn. This paper presents preliminary design analysis of biopsy needles and data from tests of a flexural needle design compared to two nonflexible designs with varying feature angles. It was hypothesized that angled flexural needles would more successfully isolate a tissue phantom and retain a larger sample when comparing the entrance resistance, entrance piercing forces, exit resistance, and the resulting sample mass of  $4\times$  scale needles.

### 2 Preliminary Design Analysis

Current biopsy needles can be classified into two main categories according to how they cut samples. End cutting needles puncture tissue using a sharpened hollow tube design to retrieve tissue. Side cutting needles use a sliding sheath to cut over an open side cavity in the needle. If either classification relies on suction to draw the sample out, the needle is termed an "aspiration needle." In all cases, a stylette prevents tissue from entering the needle until desired and can be used to remove tissue once a sample is acquired. This section details evaluation of current designs, and a first order analysis of the effective cutting ability for two general

Manuscript received May 19, 2006; final manuscript received July 28, 2006. Review conducted by Just Herder.

cutting methods. Also presented are potential strategies for cutting that could meet design specifications, which are then followed by three coring concepts.

**2.1 Performance of Existing Needle Types.** Initial design work focused on evaluation of current endoscopic biopsy designs and alternative strategies for improving tissue collection reliability. Two core endoscopic biopsy needles, one end-cut and one side-cut, as well as a side-cut percutaneous biopsy needle were used to gain an understanding of current technology and the limitations of existing designs. This qualitative comparison allowed for the assessment of overall end-cutting and side-cutting ability.

This analysis suggested that side-cut needles sometimes push tissue aside rather than cut through samples. Reasons can be the lack of cutting speed, surface tension, and large radius of curvature of the tissue sample. End-cut needles that cored out a section of tissue were effective in cutting around the circumference of a sample, but they had no reliable feature that could then sever perpendicular to the cylindrical core. This resulted in a cylindrical cut at the tissue site, but sometimes no sample in the needle.

**2.2 General Cutting Strategies.** Following this design evaluation, first order estimates of the radial stresses and axial stresses during sample gathering were used to compare the strategies (Fig. 2).

The difference between an active and a passive device was that the passive device used a radial force to sever tissue while the active devices would shear tissue. The end-cut strategy cut through the circular area  $(\pi D^2/4)$  of the tissue sample, whereas the side-cut would have to sever through an area  $\ell^*D$ , where the length  $(\ell)$  of the sample was  $\ell \approx 10D$ . In addition, passive methods would have to tear tissue in such a way that the tissue does not slip out of the needle before it is torn.

The strategy with the minimum applied force that a feature would have to produce from this estimate suggested the active end-cut had to shear the least to obtain a tissue sample. This was not surprising, since an active end-cut would shear through a smaller cross section than a side-cut device that cuts along the length of the sample. The authors hypothesized that a device that allowed tissue to enter the needle with little resistance but prevented tissue from exiting the needle by increasing resistance

Functional	Design Specifications					
Requirements						
Fit within an	Minimum endoscope channel diameter:					
endoscope to reach	2.0mm (Hitachi <sup>3</sup> )					
desired sampling	Endoscopic biopsy needle outer diameter:					
site.	1.06mm (19 Gauge) (Brugge <sup>4</sup> )					
	Needle length: 138-140mm. (5cm past					
	endoscope tube length) (Wilson-Cook <sup>5</sup> )					
	Maximum bending radius approximately					
	5cm at tip. (Pentax Model)					
Capable of Cutting	Cutting force greater than 5N. (Okamura <sup>6</sup> )					
Human Tissue	Tip buckling force of >9N when extended.					
(Stomach, Liver,	Provide a sample of approximately 15mm in					
Kidney, Pancreas)	length. (Bravo <sup>7</sup> )					
Accurate and	Cut only when at sampling site.					
Reliable	Preserve tissue histology and quality					
	Sampling Success Rate of 80% (Brugge <sup>4</sup> )					
Interface/Feedback	Compatible with standard controls					
	procedure for similar devices.					
	Tip visible under ultrasound.					

Fig. 1 Functional requirements of endoscopic biopsy needle

could act as a one-way valve to trap tissue. Concepts for an endcutting needle built upon the idea of directional resistance features.

- **2.3 Evaluation of Needle Concepts.** Following the end-cut strategy with differing entrance and exit resistances, focused group-brainstorming exercises produced over twenty designs that were evaluated for effectiveness and manufacturability [8]. The three concepts below were developed and tested:
- (i) A barbed needle with small internal features along the needle tip length that pointed radially inward. These barbs were also angled acutely into the needle such that a sample would be torn from the tissue when pulled out of the patient. Inner features could be made using a punch method, with the outside needle wall covered by a plastic sheath to prevent tissue from escaping.
- (ii) A leaflet design consisting of a single ring of angled flexures that were intended to bend towards the needle wall so that tissue could enter when inserted into the patient. When pulled out of a lesion, these same flexures would bend towards the center of the needle to sever a sample within the needle.
- (iii) A tweezers concept where a set of prongs compressed within the sheath of the needle. Once at the site of suspect tissue, the tweezers could be forced out of the sheath where the flexural prongs would expand to their unconfined shape. The sharpened end and inner lip on each prong severed tissue and the device captured a sample as the tweezers were pulled back into the sheath.

In order to test these needle concepts,  $4\times$  scale parts were made by stereolithography (SLA) and tested on a gelatin phantom as is described in more detail in Sec. 4.3. Tests revealed that the flexural design produced the highest quality samples, followed by the barbed needle concept. These observations, in addition to concerns regarding the manufacturing of small directional inner features, lead to the final concept of the biopsy needle with internal flexures.

### 3 Flexural Needle Design Principles

To design the flexural features, critical design parameters were identified to be flexure thickness (h), number of flexures (n), and the angle between the flexure and the needle wall  $(\theta)$ . In addition, the needle material's Young's Modulus (E) was considered an important factor, but this could be addressed for metal needles or even plastic needles, at a later time. The flexure thickness h would be approximately the same thickness as the needle wall for a metal design and possibly thicker for a plastic needle [9]. The flexure width b was approximately the circumference of the needle divided by the number of flexures at its base and would

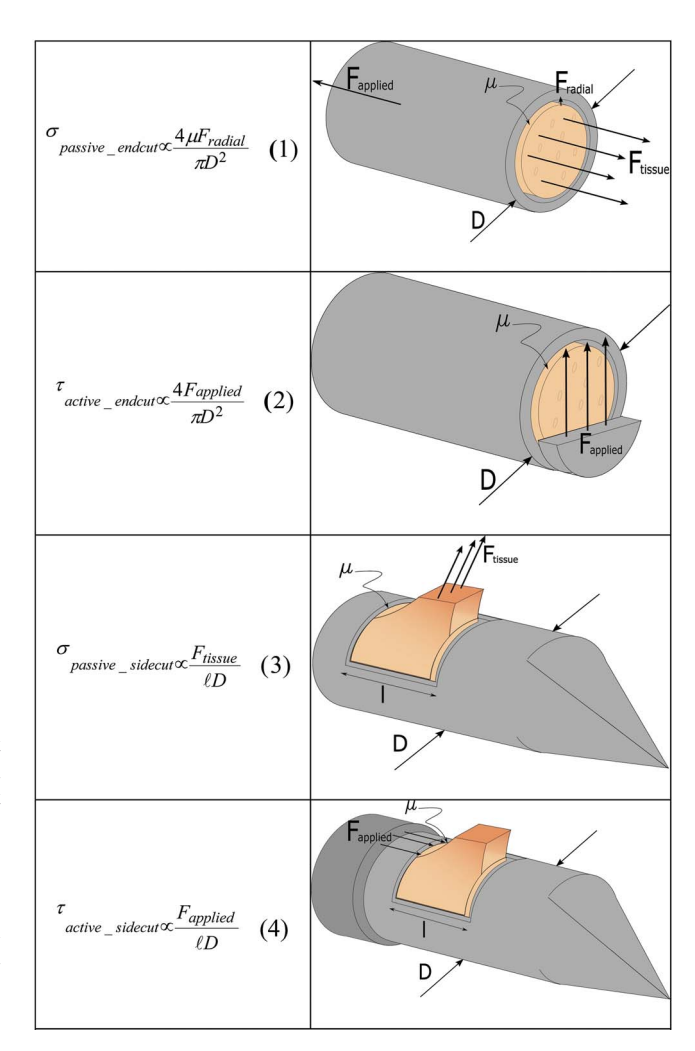


Fig. 2 First-order estimates of cutting force and cutting strategies

have to narrow as it approaches the center of the needle to prevent interference. The length of the flexure l was limited to the product of half the inner diameter of the needle and  $\sin(\theta)$ . The tip deflection d of the flexure (assuming small deflections and a distributed load) was calculated from these values where the angle of the flexure changes depending on the direction of the applied force. The equations below provide a first-order estimate of the flexural needle forces and the tip deflection of each flexural member

$$F_{\text{entrance\_normal}} \approx \frac{F_{\text{applied}}}{n} \sin(\theta - \delta\theta)$$
 (5)

$$F_{\text{exit\_normal}} \approx \frac{F_{\text{applied}}}{n} \sin(\theta + \delta\theta)$$
 (6)

$$I_x = \frac{bh^3}{12} \tag{7}$$

$$d = \frac{F_{\text{normal}}\ell^3}{8EI} \tag{8}$$

Using design of experiments (DOE) techniques [10], a  $3 \times 3$  orthogonal array experiment was developed to determine a parameter configuration that would give the best biopsy performance by providing the longest and most intact tissue core sample. This preliminary data suggested that a needle with four flexures and a 45 deg angle to the inner wall was the most effective, with a

30 deg angle also more effective than a 60 deg angle. The best thickness for the flexures was inconclusive, which was considered to be due to limitations of the SLA thickness.

While the preliminary tests for flexure parameters proved useful, the small sample size (four samples for each of nine variations), critical nature of the design, and FEA analysis of the bending stresses, suggested further testing was appropriate.

# 4 Procedure and Testing of 10× Scale Needles

In order to test the performance of the leaflet geometry more rigorously, a set of stereolithographed parts were designed that allowed scaling of parameters. These prototypes were tested using a TA.XTPlus Texture Analyzer (Texture Technologies Corp., Scarsdale, NY/Stable Micro Systems, Godalming, Surrey, UK) to obtain force deflection curves for the designs when pierced into a gelatin tissue phanton. Data collected from the needle tests included force displacement curves for each sample and sample mass for each randomly assigned needle letter. For each curve the piercing force, peak entrance force, entrance slope and exit slope were obtained, as described in Sec. 5.1. A lower entrance resistance (S1), higher exit resistance (S2), and a lower peak force (P2) would be desirable to obtain a gelatin sample. The piercing force (P1), entrance resistance of pre-pierced site (S1') and exit resistance of pre-pierced site (S2') should not depend on which needle is used. Finally, sample mass to feature type and feature angle data was gathered to look at how parameters may affect tissue gathering ability.

**4.1 Needle Variations.** To test the tissue capture ability of the flexures as compared to a nonflexible member design, a wedge design was introduced. This wedge had the same overall angle as a flexure, but lacked the ability to deform when in contact with tissue. This could present itself as a simpler design that would lend itself to the benefits of injection molding. This extended wedge design was also introduced with angular variations and an extended section immediately following the wedge shape, which was meant to test whether the full wedge angle was significant in collecting tissue. Cross-sectional views of the needle variations tested are shown in Fig. 3. A 4× coring needle with no inner features (not shown) was used to obtain a small number of samples during the force-deflection tests.

**4.2** Scaling of Needle Tip Prototypes. To verify dimensional parameters of the flexural needle design, a second set of prototype needles were also produced using a stereolithography process. Due to the resolution of this manufacturing process, which was limited to about 0.01 in. (0.25 mm) in the z-direction (build direction) and 0.003 in. (0.09 mm) in plane of the process [11] the needles were scaled so their critical inner feature was approximately 10 times the best SLA resolution. Dimensions were determined by matching the bending modulus (EI) for the scale needle using an approximation of  $E_{\rm sla}$ =4.5×10<sup>9</sup> Pa for the stereolithographed parts and  $E_{\rm stainless\_steel}$ =200×10<sup>9</sup> Pa. Here L is the length of the needle cantilevered out of the endoscope

$$F_{\text{buckling}} > F_{\text{applied}}$$
 (9)

$$F_{\text{buckling}} = \frac{\pi^2 E I_{\text{needle\_wall}}}{4 L^2}$$
 (10)

$$I_{\text{needle\_wall}} = \frac{\pi}{4} (R_0^4 - R_i^4)$$
 (11)

By using the minimum resolution of the needle to set the inner radius  $R_i$ , and assuming an applied force of 5 N, one can then match the I and E for the prototype to that of a stainless steel needle. This buckling equation assumes that the flexures are not cut from the needle wall, which would lower the overall buckling force, but this can be addressed by adjusting the cantilever length and inner diameter of the needle on the  $1 \times$  scale.

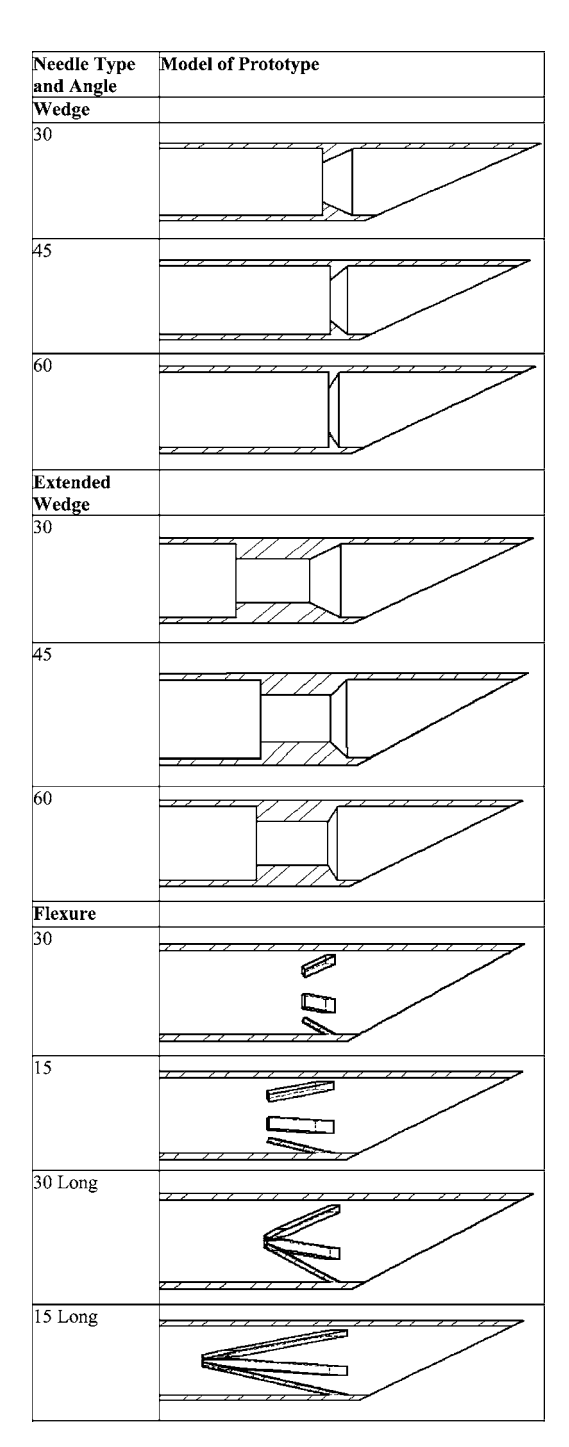


Fig. 3 Needle prototype cross-sections

4.3 Tissue Phantom for 10× Scale Needles. In order to approximate realistic tissue deflection and compression properties for the unsharpened SLA needle designs on a 10× scale, a test material was needed that would deform more readily than actual tissue. A gelatin phantom was chosen for its relatively stable consistency at room temperature, and its shear and compressive properties that behave similarly to actual tissue [12]. The Young's modulus for gelatin has been shown to vary depending on pH, concentration, and loading frequency, with an estimate of 3.6 kPa for 10% gelatin phantoms [13].

Yamada et al. estimate the Young's Modulus of liver tissue around 30 kPa, with other references giving 59 kPa [14,15]. References for the Poisson's ratio of porcine liver suggest  $0.47\pm0.15$  for elongation and  $0.43\pm0.15$  for compression [16]. A yield stress

Table 1 Entrance and exit characteristics of sample needles (\*\* indicates data not available)

Туре	Angle	S1 (g/mm)	Std Dev	S2 (g/mm)	Std Dev	S1' (g/mm)	Std Dev	S2' (g/mm)	Std Dev	P1 (g)	Std Dev	P2 (g)	Std Dev
Standard Core	none	4.1	0.1	-1.75	0.7	**	**	**	**	56	10.5	59	4.41
Extended Wedge	30	7.0	**	-0.5	**	1.9	0.2	-1.7	0.3	60	**	400	**
Extended Wedge	45	7.4	0.3	-1.0	1.0	0.9	0.1	-2.3	0.4	52	5.1	349	20.8
Extended Wedge	60	6.7	0.8	-0.1	0.7	2.2	0.3	-1.8	0.1	61	20.4	335	55.7
Flexure	15	7.5	0.5	-7.3	2.0	2.1	0.4	-1.3	0.2	63	7.9	187	45.0
Flexure	15	6.8	0.5	-3.5	2.2	2.2	0.5	-1.8	0.5	96	33.2	155	16.3
Flexure	30	5.2	0.3	-2.5	1.5	2.2	0.2	-4.4	1.0	129	18.7	173	21.0
Flexure	30	4.6	0.3	-2.6	1.6	1.9	0.2	-2.2	0.2	46	10.3	103	40.2
Wedge	30	7.1	0.6	-0.8	1.2	2.5	**	-2.5	**	79	13.3	316	24.6
Wedge	45	9.1	0.9	-3.0	2.6	3.4	0.4	-2.5	0.2	48	6.1	426	48.1
Wedge	60	5.9	0.6	-4.6	1.3	2.2	0.3	-3.7	0.2	130	13.3	240	34.6

of  $2.5 \times 10^5$  Pa was also found in the literature [16]. These material properties may vary depending on frequency of the applied force, cutting speed, and because of inherent inhomogeneous properties of liver due to location and donor specimen condition.

Hertz contact estimates of the maximum shear stress  $\tau_{\rm max}$  allow one to compare the force (P) required to yield the samples by using an effective Young's modulus  $E^*$  to estimate deflection of both the needle and the tissue material. With the relative curvature of the contact surfaces (1/R) approximated using R equal to half the wall thickness, the following equation was used [17]:

$$\tau_{\text{max}} = 0.3 \left( \frac{PE^*}{\pi R} \right)^{1/2} \tag{12}$$

For the case of a  $1\times$  stainless steel needle and a  $10\times$  SLA prototype

$$\tau_{\text{max stainless steel}} = 1600 \text{ Pa}$$
 (13)

$$\tau_{\text{max SLA prototype}} = 900 \text{ Pa}$$
 (14)

**4.4 Force Displacement Testing Setup.** The eleven needle variations were randomly labeled and were tested using a TA.XTPlus with a 5 kg load cell that was capable of measuring forces to within 0.1 g. Each needle variation was plunged into a gelatin mixture that was prepared according to Knox Gelatine instructions [18], replacing juice with water, and allowed to cool for a minimum of 18 h at 23.5 °C as suggested [19]. Each prototype variation was cycled 40 mm into the gelatin at a rate of 4.5 mm/s and then extracted fully out of the phantom tissue. This was repeated ten times, each time at a new site approximately three needle-diameters center to center from the previous site, while measuring force and displacement of both the plunging and extracting movements. A standard coring needle with no inner features was used to obtain three samples for comparison of force and slope data.

In order to subtract the friction that occurred on the outer wall of each needle, which would not be influenced by the internal features of either design, each needle was inserted into a previously punctured gelatin cavity while measuring force and displacement. Finally, the initial mass and final mass of the needles were measured to record the mass of gelatin that was captured for each sample.

The needle designs were then evaluated based on their average mass of sample captured as a function of type (flexure, wedge, or extended wedge) as well as feature angle, which were 15, 30, 45, or 60 deg relative to the needle wall.

# 5 Results

Presented below is data collected from the force displacement and sample mass tests, including standard deviations of the data summarized in Table 1. **5.1 Force Displacement Data Results.** Force displacement curves were compared according to the overall shape by characterizing the piercing slope S1 (g/mm), the extraction slope in the region of tissue tearing S2 (g/mm), puncture force P1 (g), and frictional peak P2 (g) as shown in Fig. 4. Similarly, the piercing slope S1' (g/mm) and extraction slope S2' (g/mm), as shown in Fig. 5, were recorded for a pre-pierced gelatin site, which would indicate frictional characteristics of the outer wall. While Okamura et al. [20] list a quadratic relationship in the puncture step, a linear best-fit curve was used for the slope in regions where possible.

# 5.2 Sample Mass Comparisons for Design Type and Angle. The average mass of sample gelatin collected by needles was compared to the feature type and feature angle to determine whether either parameter affected tissue collection. The number of

whether either parameter affected tissue collection. The number of the design for a particular design type was plotted in addition to the testing parameters and the number of each design that was prototyped so trends for each design were more evident. One particularly successful test of this flexural design at  $10 \times$  scale is shown in Fig. 6.

### 6 Discussion

The analysis of internal features for an endoscopic biopsy needle compared to average sample mass is shown in Figs. 7 and 8 according to feature type and angle. The average mass of a sample for a flexural needle design was 1.1 g ( $\sigma$ =0.21) compared to 0.78 g ( $\sigma$ =0.19) for a wedge design and 0.71 g ( $\sigma$ =0.09) for the extended wedge. It was also shown that the average sample mass was 1.1 g ( $\sigma$ =0.08) for a 15 deg needle, 0.95 g ( $\sigma$ =0.08) for the 30 deg needles, 0.77 g ( $\sigma$ =0.04) for the 45 deg needles, and 0.61 g ( $\sigma$ =0.05) for the 60 deg needles. The increase in sample mass with smaller angle and better results for a flexure suggests that the sample mass would be highest for a 15 deg flexural needle.

Force displacement results for the needle prototypes exhibited curves with a maximum piercing force of approximately 3 N (300 g), which scaled to the same order of magnitude of the target max applied force of 5 N, and fit within previously documented range for actual needle piercing experiments. So, the scaling appeared to be correct for the 10× needle and gelatin, which emulated actual size needles and tissue. The range of the peak piercing forces P1 from 0.44 to 1.47 N (45–150 g) estimated the 1 N forces referenced by Okamura, and was close enough that it could be adjusted by altering the gelatin concentrations (Fig. 9). The peak of the friction curve P2 had a dependence on the internal features. The lower peak for flexural designs as compared to wedge designs and the extended wedge indicated that the flexures did in fact exhibit a lower entrance resistance than either the

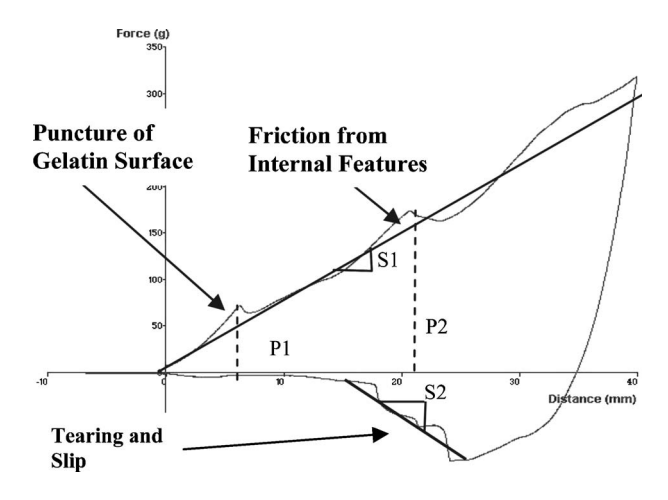


Fig. 4 Force displacement curve for a flexural design with characteristic drop during needle puncture and sharp decrease in force during tissue tearing. Peaks from piercing and design features are also present.

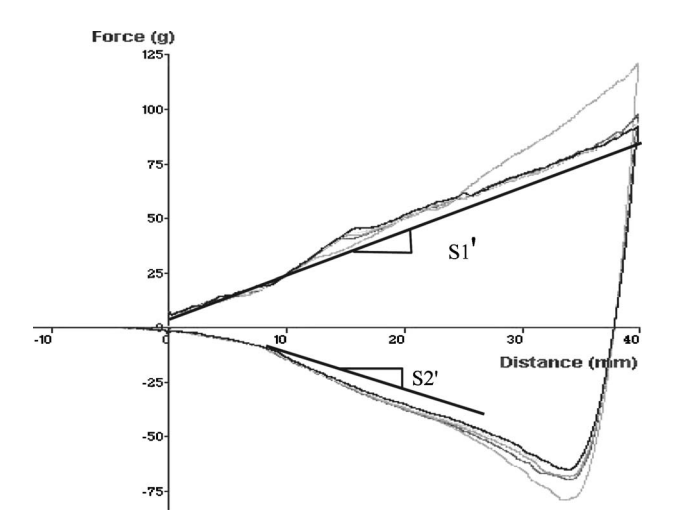
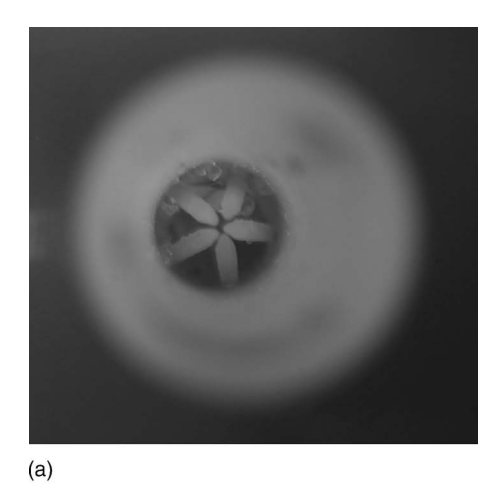


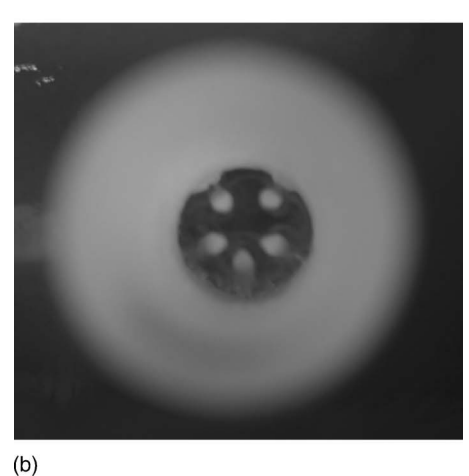
Fig. 5 Force displacement curve of pre-pierced site showing slope from friction of outer wall, which is estimated using a linear best-fit approximation

wedge or extended wedge designs. The piercing peak P1, as would be expected, exhibited no dependence on the needle type.

Also evident from the peak values of the curves in Fig. 10 is the relationship between angle and peak friction force P2. As the angle increased, the frictional force increased for the needle sample. This matches the relationship described in Eq. (5), although the major improvement in peak friction was seen between 30 deg with an average force of 1.9 N (198 g)  $\sigma$ =28 and 45 deg with an average of 3.8 N (388 g) and  $\sigma$ =34, which is significant. As expected, there was no marked relationship between the internal feature angle and the puncture force P1.

The slope of the force displacement curves during puncture S1 showed only a slight dependence on the needle type, as seen in Figs. 11 and from the standard deviations in column 4 of Table 1. This relationship was most likely a result of the characteristic peaks for each needle type weighing into the linear best-fit curve and not a direct result of the internal feature. This result is also supported by the idea that the linear curve is an estimation of wall friction, as described by Simone and Okamura [20] and the punc-





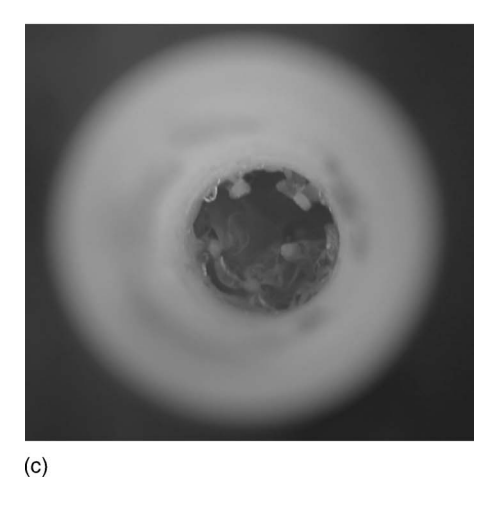


Fig. 6 Flexure deformation sequence while entering gelatin during test. (a) Piercing, (b) initial entrance, and (c) sample collected prior to withdrawal and severing.

ture force more closely fit a quadratic polynomial. Further, there was no effect on the slope of the pre-pierced site S1' as needle type varies, which was expected.

A relationship that was evident was the effect of needle type on the slope of the needle exit curves S2 in Fig. 11. The flexure designs showed a larger magnitude slope of -4.0 g/mm, followed by the wedge -2.8 g/mm and the extended wedge -0.6 g/mm designs. This abrupt change in force corresponded to a sudden failure in the gelatin, which was observed during testing, as opposed to a gradual sliding of the sample. This result suggests an

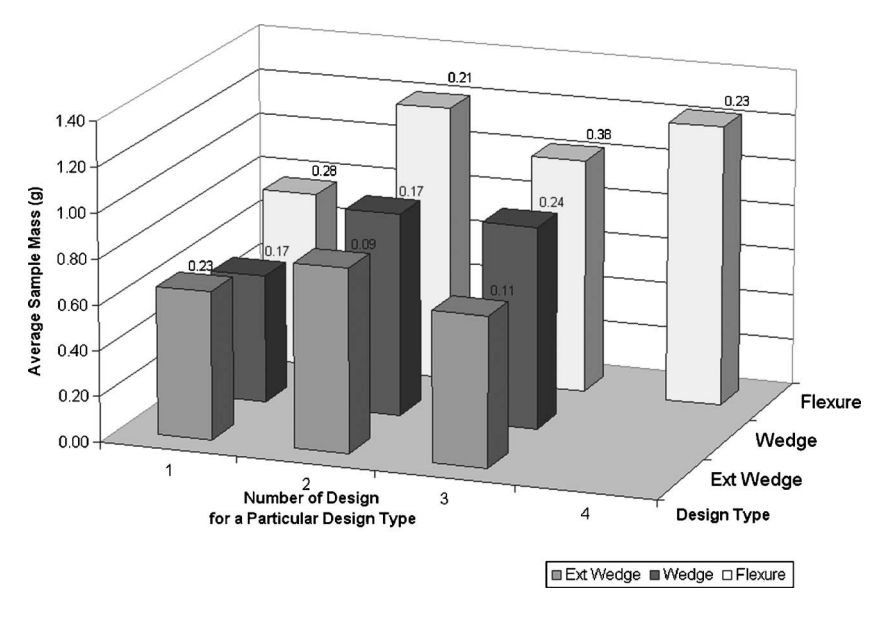


Fig. 7 Average sample mass (g) versus design type with a sample size of 10. Standard deviation noted above each data set.

increased likelihood of successfully severing a tissue sample, although the average standard deviation ( $\sigma$ =1.5) was rather high and would benefit from a larger sampling of needles.

The angle of the needle entrance created no noticeable difference in S1 and S1' (Fig. 12). This corresponds with previous comments suggesting the linear slope is related to wall friction, with piercing causing a quadratic peak.

There was a relationship between the exit slope S2 and angle, as was hypothesized. As the feature angle increased, exit slope decreased, which suggests that there was less tissue captured, and is also supported by the mass results reported previously. The inner feature angle had no effect on the slope of the exit curve in the pre-pierced case S1'.

## 7 Conclusions and Future Work

The analysis of sample mass and force-deflection curves for the design of the proposed new endoscopic biopsy needle suggests that internal flexural features are an effective method of capturing tissue. Increase in sample mass was achieved by maintaining a low entrance resistance, but introducing a significant exit resistance to tissue. In particular, low angle (15 and 30 deg) flexures were the most effective method for tissue sampling according to sample mass and frictional force-displacement analysis.

Future steps to realize this design in a product would include the manufacture of these features on actual 19 gauge stainless steel needles and molded plastic needles. This would allow for

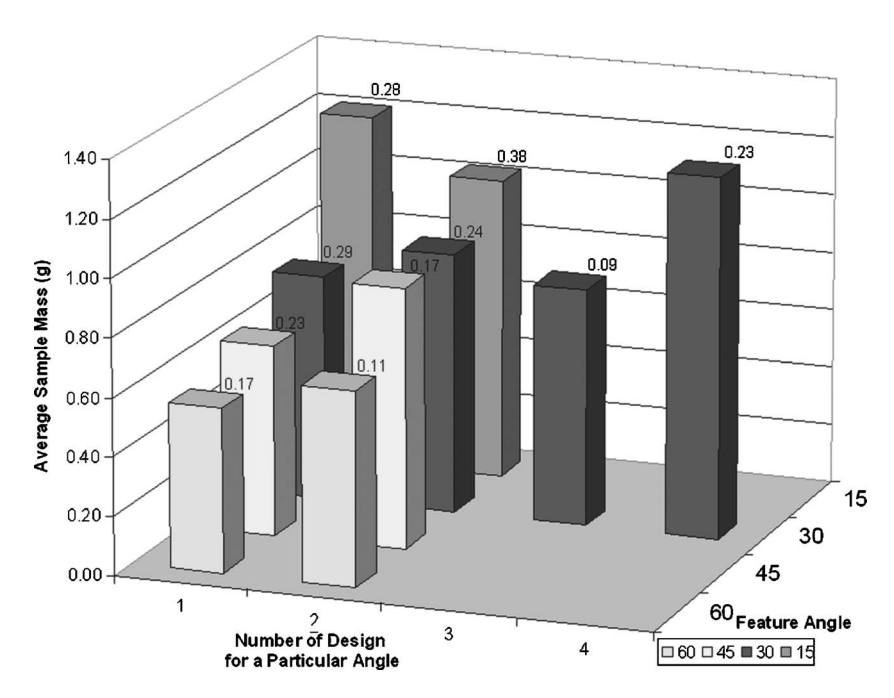


Fig. 8 Average sample mass (g) versus feature angle (degrees) with a sample size of 10. Standard deviation noted above each data set.

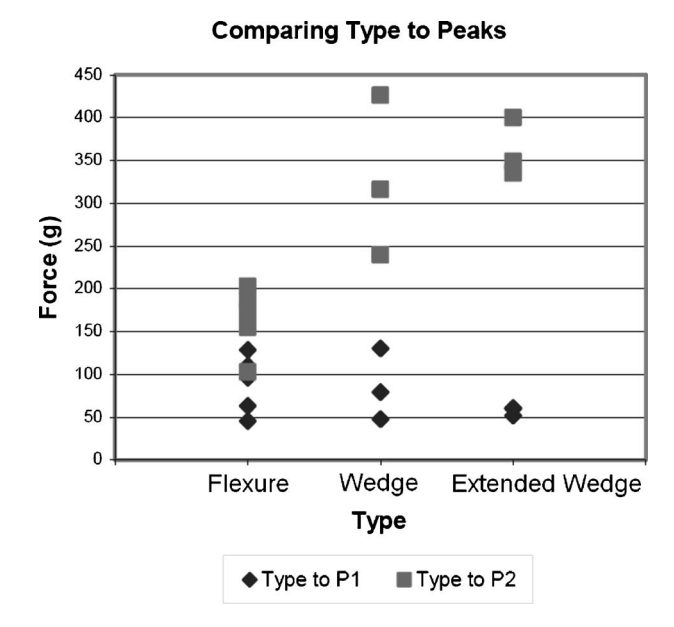


Fig. 9 Comparison of design type to characteristic peaks

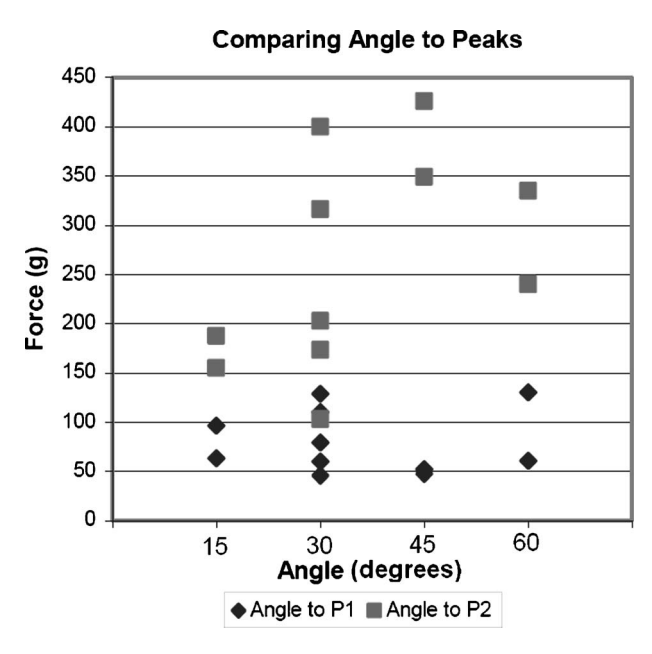


Fig. 10 Comparison of feature angle to characteristic peaks

comparison using actual tissue on the  $1\times$  scale, and it would enable direct comparison with endoscopic biopsy needles that are currently used. It would also help to overcome the manufacturing challenges of producing such small features on a needle, which the authors expect would initially be laser cut into a standard stainless steel needle wall and bent to the desired angle. A patent is currently pending on these new biopsy needle designs.

# Acknowledgment

The authors would like to thank the other individuals who contributed to initial research, concept generation, and analysis during MIT course 2.75 Precision Machine Design: Andrew Carvey, Bill Fienup, Barry Kudrowitz, and Jacob Wronksi. We appreciate the help of Professor Mary Boyce and Asha Balakrishnan for use of their lab and assistance with the TA.XTPlus setup and data acquisition. We are also grateful to Massachusetts General Hospital for

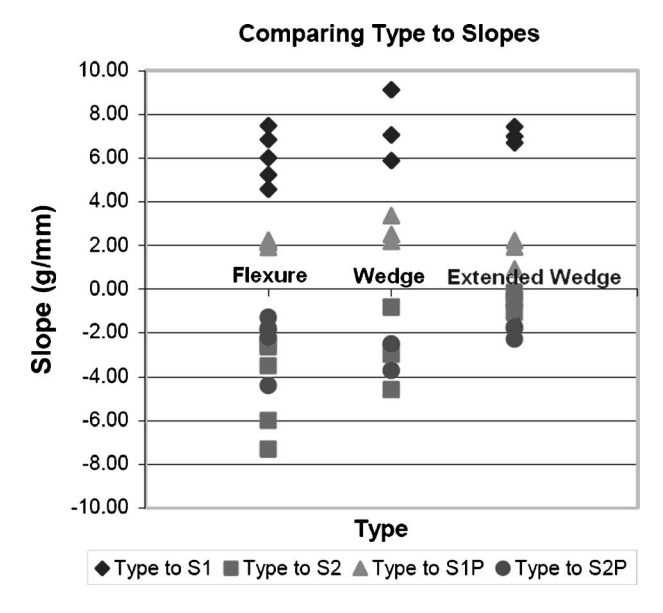


Fig. 11 Relationship between feature type and characteristic slopes

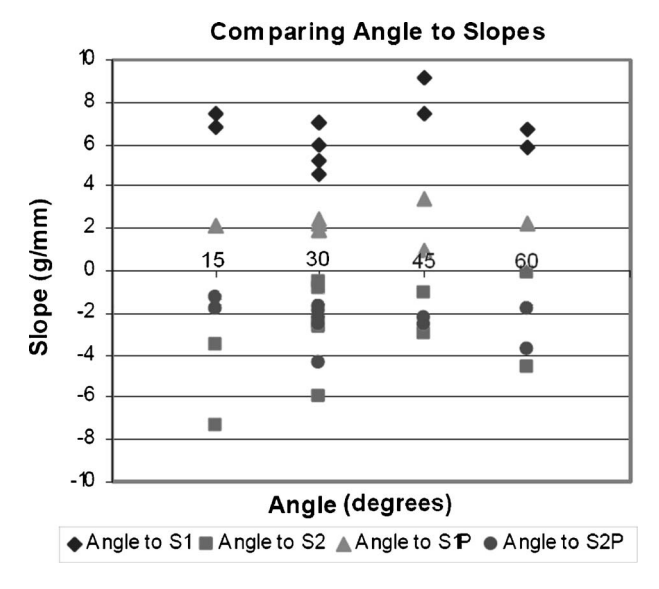


Fig. 12 Comparison of feature angle to characteristic slope

use of their facilities and excellent staff. The Center for Integration of Medicine and Innovative Technology (www.cimit.org) has supported this project with funding provided from the U.S. Army Medical Acquisition Activity (USAMRAA) under cooperative agreement No. DAMD 17-02-2-0006. The content of this information does not necessarily reflect the position or policy of the Government, and no official endorsement should be inferred.

# References

- [1] Pohl, H., and Welch, H. G., 2005, "The Role of Overdiagnosis and Reclassification in the Marked Increase of Esophageal Adenocarcinoma Incidence." J. Natl. Cancer Inst., 97(2), pp. 142–146.
- [2] National Center for Health Statistics, 1998, "Ambulatory and Inpatient Procedures in the United States, 1996," Vital and Health Statistics, Series 13, No. 139.
- [3] Hitachi, Model FG-34UX, http://www.hitachi-medical-systems.com/us\_probsys\_probes.php?proID=4.
- [4] Brugge, W. R., 2004, personal communication.
- [5] Cook Endoscopy, Model EUSN-20-CPN, http://www.cookendoscopy.com/esoph/ultrasound/usn04.html.
- [6] Okamura, A. M., Simone, C., and O'Leary, M. D., 2004, "Force Modeling for

- Needle Insertion Into Soft Tissue," IEEE Trans. Biomed. Eng., 51(10), p.
- [7] Bravo, A. A., Sheth, S. G., and Chopra, S., 2001, "Liver Biopsy," N. Engl. J. Med., 344, pp. 495-500.
- [8] Figueredo, S., 2006, Design of an Endoscopic Biopsy Needle With Flexural Members, SM thesis, MIT.
- [9] Avallone, E. A., and Baumeister, T., III, 1996, Marks' Standard Handbook for Mechanical Engineers, 10th ed., McGraw-Hill, New York, pp. 5-23.
- [10] Antony, J., 2003, Design of Experiments for Engineers and Scientists, Butterworth-Heinemann, Oxford.
- [11] Mostovoy, G., 2005, personal communication.[12] Leiner, P. B., "Physical and Chemical Properties of Gelatin," www.gelatin.com.
- [13] Erpelding, T. N., Booi, R. C., Hollman, K. W., and O'Donnell, M., 2003, "Measuring Tissue Elastic Properties Using Acoustic Radiation Force on Laser-Generated Bubbles," IEEE Ultrasonics Symposium.

- [14] Yamada, H., 1970, Strength of Biological Materials, Williams and Wilkins, Baltimore
- [15] Chanthasopeephan, T., Desai, J., and Lau, A., 2003, "Measuring Forces in Liver Cutting: New Equipment and Experimental Results." Ann. Biomed. Eng., 31, pp. 1372-1382.
- [16] Chui, C., Kobayashi, E., Chen, X., Hisada, T., and Sakuma, I., 2004, "Combined Compression and Elongation Experiments and Nonlinear Modeling of Liver Tissue for Surgical Simulation." Med. Biol. Eng. Comput., 42, pp. 787-
- [17] Johnson, K. L., 1985, Contact Mechanics, Cambridge University Press, Cam-
- [18] Kraft Foods, www.kraftfoods.com/knox.
- [19] Leiner, P. B., "Preparing Gelatin Solutions," www.gelatin.com.
- [20] Simone, C., and Okamura, A. M., 2002, "Modeling of Needle Insertion Forces for Robot-Assisted Percutaneous Therapy," IEEE International Conference on Robotics Automation, pp. 2085-2091.

8 / Vol. 1, MARCH 2007 Transactions of the ASME